

# Linköping University Post Print

## **Evaluation of a lithium formate EPR dosimetry system for dose measurements around Ir-192 brachytherapy sources**

Laura Antonovic, Håkan Gustafsson, Gudrun Alm Carlsson and Åsa Carlsson Tedgren

N.B.: When citing this work, cite the original article.

Original Publication:

Laura Antonovic, Håkan Gustafsson, Gudrun Alm Carlsson and Åsa Carlsson Tedgren, Evaluation of a lithium formate EPR dosimetry system for dose measurements around Ir-192 brachytherapy sources, 2009, MEDICAL PHYSICS, (36), 6, 2236-2247.

<http://dx.doi.org/10.1118/1.3110068>

Copyright: American Institute of Physics

<http://www.aip.org/>

Postprint available at: Linköping University Electronic Press

<http://urn.kb.se/resolve?urn=urn:nbn:se:liu:diva-19422>

# Evaluation of a lithium formate EPR dosimetry system for dose measurements around $^{192}\text{Ir}$ brachytherapy sources

Laura Antonovic, Håkan Gustafsson, Gudrun Alm Carlsson, and Åsa Carlsson Tedgren<sup>a)</sup>  
*Department of Medical and Health Sciences (IMH), Radiation Physics, Faculty of Health Sciences,  
Linköping University, SE-581 85 Linköping, Sweden*

(Received 27 September 2008; revised 9 March 2009; accepted for publication 10 March 2009;  
published 18 May 2009)

A dosimetry system using lithium formate monohydrate ( $\text{HCO}_2\text{Li}\cdot\text{H}_2\text{O}$ ) as detector material and electron paramagnetic resonance (EPR) spectroscopy for readout has been used to measure absorbed dose distributions around clinical  $^{192}\text{Ir}$  sources. Cylindrical tablets with diameter of 4.5 mm, height of 4.8 mm, and density of  $1.26\text{ g/cm}^3$  were manufactured. Homogeneity test and calibration of the dosimeters were performed in a 6 MV photon beam.  $^{192}\text{Ir}$  irradiations were performed in a PMMA phantom using two different source models, the GammaMed Plus HDR and the microSelectron PDR-v1 model. Measured absorbed doses to water in the PMMA phantom were converted to the corresponding absorbed doses to water in water phantoms of dimensions used by the treatment planning systems (TPSs) using correction factors explicitly derived for this experiment. Experimentally determined absorbed doses agreed with the absorbed doses to water calculated by the TPS to within  $\pm 2.9\%$ . Relative standard uncertainties in the experimentally determined absorbed doses were estimated to be within the range of 1.7%–1.3% depending on the radial distance from the source, the type of source (HDR or PDR), and the particular absorbed doses used. This work shows that a lithium formate dosimetry system is well suited for measurements of absorbed dose to water around clinical HDR and PDR  $^{192}\text{Ir}$  sources. Being less energy dependent than the commonly used thermoluminescent lithium fluoride (LiF) dosimeters, lithium formate monohydrate dosimeters are well suited to measure absorbed doses in situations where the energy dependence cannot easily be accounted for such as in multiple-source irradiations to verify treatment plans. Their wide dynamic range and linear dose response over the dose interval of 0.2–1000 Gy make them suitable for measurements on sources of the strengths used in clinical applications. The dosimeter size needs, however, to be reduced for application to single-source dosimetry. © 2009 American Association of Physicists in Medicine. [DOI: 10.1118/1.3110068]

Key words: experimental  $^{192}\text{Ir}$  dosimetry, electron paramagnetic resonance detector

## I. INTRODUCTION

Interest in experimental  $^{192}\text{Ir}$  dosimetry has increased and recent applications include the development of detectors suitable for *in vivo* dosimetry<sup>1</sup> and for verifying the doses calculated by treatment planning systems (TPSs).<sup>2</sup> Dose calculation in treatment planning of brachytherapy is based on the superposition of precalculated single-source dose distributions in water<sup>3</sup> which is why the distributions must be well characterized before a new  $^{192}\text{Ir}$  source model can be clinically used. To this end, the American Association of Physicists in Medicine (AAPM) recommends use of the brachytherapy dose calculation formalism presented in Task Group 43 (TG43U1) report.<sup>3</sup> This is primarily concerned with low-energy seeds and, for these, both an experimental and a Monte Carlo study for each new type of source should be performed. For new sources of the more energetic  $^{192}\text{Ir}$  isotope, either an experimental or a Monte Carlo (MC) characterization is recommended.<sup>4</sup>

Dose gradients around  $^{192}\text{Ir}$  brachytherapy sources are steep and small dosimeters are needed to resolve them. In addition, the photon energy spectrum varies significantly with depth so that dosimeters with a low-energy dependence relative to water (the reference medium for brachytherapy

dosimetry) are desirable. Furthermore, the dosimeters should be able to respond linearly over a large range of absorbed dose and dose rate values. The most common dosimetry system for brachytherapy uses thermoluminescent (TL) dosimeters of lithium fluoride (LiF).<sup>5–7</sup> However, while such dosimeters can be made small enough for resolving steep dose gradients, they have several drawbacks. Their energy dependence relative to water is relatively strong, the dose range within which the response is linear is fairly small, and they may exhibit a LET dependence.<sup>8,9</sup> For low-energy (<50 keV) photon-emitting single brachytherapy sources, the combined relative standard uncertainty in experimental data is typically about 8%,<sup>3</sup> while for  $^{192}\text{Ir}$  the corresponding figure is 6%–7%.<sup>10</sup>

Alanine, the most common material in electron paramagnetic resonance (EPR) dosimetry, has been used for measurements around  $^{192}\text{Ir}$  brachytherapy sources.<sup>11–13</sup> A drawback of EPR dosimetry is the need for high doses (above around 1–2 Gy) while an advantage is the system's linear response over a large dose interval<sup>14</sup> making it easy to measure doses around pulsed dose rate (PDR) and high dose rate (HDR)  $^{192}\text{Ir}$  sources at their clinical strength. The verification of doses at several distances from an implant with a single ir-

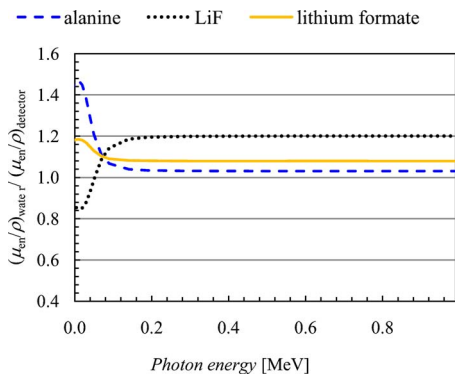


FIG. 1. Mass-energy absorption coefficients of water relative to LiF, alanine, and lithium formate for monoenergetic photons.

radiation will not be a problem and doses large enough for the source transit dose<sup>15–17</sup> to be negligible can easily be administered. Due to problems with supralinearity, TL dosimeters close to the source must often be withdrawn before ones at larger distances. Early reports on TL dosimetry for  $^{192}\text{Ir}$  was for low dose rate (LDR) seeds<sup>7</sup> and TL dosimetry around  $^{192}\text{Ir}$  HDR and PDR sources is mostly made with decayed sources.<sup>10,18</sup>

In experimental verifications of treatment plans, it is not possible to perform corrections due to changes in photon-energy spectra since these are unknown for an arbitrary multiple-source implant. It is thus of interest to have access to a dosimetry system with little dependence on energy. Lithium formate monohydrate is currently one of the most promising materials for EPR dosimetry. Depending on read-out procedure, lithium formate is two to six times more sensitive<sup>19,20</sup> than alanine. Furthermore, at energies below 200 keV the energy absorption characteristics of lithium formate are more similar to water than those of alanine and LiF. Figure 1 presents the mass-energy absorption coefficients of water relative to LiF, alanine, and lithium formate for monoenergetic photons. As can be seen, the ratio varies substantially less at low energies for lithium formate than for the other detector materials.

The radiation induced radicals in lithium formate are well characterized,<sup>21</sup> the dose response was found to be linear over a large dose range (0.2–1000 Gy),<sup>20</sup> and no signal fading was observed for at least 28 days.<sup>19</sup> Lithium formate EPR dosimetry has been compared with LiF TL dosimetry<sup>22</sup> and been used, for example, in measurements in high-energy electron beams.<sup>23</sup> Gustafsson *et al.*<sup>24</sup> recently applied lithium formate dosimeters to verify planned IMRT doses.

The aim of the present work was to evaluate the performance of a lithium formate monohydrate EPR dosimetry system<sup>19,24</sup> (from now on called the lithium formate dosimetry system) for measurements around  $^{192}\text{Ir}$  brachytherapy sources.

## II. MATERIALS AND METHODS

### II.A. The lithium formate dosimetry system

The lithium formate dosimetry system summarized below is the same system as that used earlier to verify planned

IMRT doses.<sup>24</sup> More details about this system are reported elsewhere.<sup>19</sup> This section starts by describing how dosimeters were manufactured (Sec. II A 1), continues with details of the EPR read-out procedure (Sec. II A 2) and the dose-response homogeneity test that all dosimeters underwent (Sec. II A 3), and ends by describing how the system was calibrated for absolute dose measurements (Sec. II A 4).

#### II.A.1. Dosimeter manufacture

The active dosimetry material “lithium formate monohydrate” ( $\text{HCO}_2\text{Li}\cdot\text{H}_2\text{O}$ ) was purchased from Aldrich. Solid household paraffin (Haugen-Gruppen AB, Norrköping, Sweden) was used as a binder (10% of dosimeter weight).

Lithium formate was crushed in a mortar. The crushed material was sieved to the grain size interval  $180\ \mu\text{m} < d < 500\ \mu\text{m}$  using an Endecotts MINOR test sieve shaker and was put in a beaker together with solid paraffin. The beaker and its content were heated in an oven until the paraffin had melted. Since paraffin has a lower melting point (54–56 °C) than lithium formate crystals (94 °C), it melts without damaging the grains. The two components were mixed thoroughly. Heating and mixing were repeated twice. Using a manual pellet press, cylindrical dosimeters of diameter 4.5 mm and height 4.8 mm were prepared from 100 mg of the mixture. Tablets outside the mass interval  $100 \pm 1$  mg were rejected. Dosimeters made from the same mixture were regarded as belonging to one batch and used together in the subsequent experiments. All dosimeters were stored in the same environmental conditions.

#### II.A.2. EPR readout

The dosimeter signal was measured using a BRUKER EleXsys E580 EPR spectrometer equipped with a standard cavity ER 4102ST. Tablets were held in a WILMAD EPR sample tube, Q-5M-6M-0–200m-FB (inner diameter of 5 mm, flat bottom), resting in the notch of an in-cavity pedestal which ensured that the tube was placed in the same position in each reading. Spectrometer settings were chosen in order to optimize the precision of repeated measurements of a single dosimeter within a reasonable time interval. As described previously<sup>19,24</sup> the highest precision was achieved for measurements with a narrow sweep width (3 mT) without using an in-cavity reference such as synthetic ruby or  $\text{Mn}^{2+}/\text{MgO}$ . The readings were thus performed using an applied microwave power of 20 mW, 3 mT sweep width, 1.2 mT modulation amplitude, 328 ms time constant, and one 168 s sweep. The EPR signal was not smoothed, filtered, or manipulated in any way. The signal amplitude was determined as the peak-to-peak height in the first derivative of the absorbance spectrum ( $I$ ) divided by the mass  $w$  of the dosimeter and was denoted  $I_w$  ( $\text{mg}^{-1}$ ). The signal amplitude for each dosimeter was defined as the average of five measurements. The sensitivity of the spectrometer varies from day to day. For this reason, all dosimeters in a batch were measured during the same day in one measurement session. In order to compensate for possible small variations in spectrometer sensitivity during a measurement session, the five readings of

each dosimeter were spread out during the day. It is well known that nonirradiated alanine EPR dosimeters, to various degrees, have a zero-dose signal due to mechanically induced radicals.<sup>25</sup> However, no mechanically induced signal was observed in nonirradiated lithium formate tablets. This is in accordance with findings by Vestad *et al.*<sup>20</sup>

### II.A.3. Dose-response homogeneity control

By using the manufacturing method described above, all dosimeters of one batch will have the same dose response (signal per unit absorbed dose) to within a certain spread depending partly on dosimeter properties such as size, density, and binder distribution and partly on spectrometer sensitivity variations. By irradiating all dosimeters to the same dose, this spread can be determined in terms of the relative standard deviation in resulting signals of one batch. All dosimeters of a batch (ten at a time for batches of 30 dosimeters) were irradiated to the same dose (at least 3 Gy) in a 6 MV photon beam (Varian Clinac 600 C/D accelerator) at 5 cm depth in a PMMA phantom using a field of area  $15 \times 15 \text{ cm}^2$  and SSD 100 cm. The sides of the PMMA phantom were  $20 \times 20 \text{ cm}^2$ , the height was 6 cm, and 8 cm back-scattering material (PMMA) was employed. To remove any influence of the slightly nonhomogeneous beam profiles (i.e., to ensure the same dose to each dosimeter independent of position within the beam) the dosimeters were rotated in the phantom so that each one was irradiated for the same time in each position. In the present work, the relative standard deviation of the signals of one whole batch, consisting of 30 dosimeters, was 0.6%. The signal corresponding to the absorbed dose in the homogeneity control irradiation is from now on regarded as the (induced) background signal.

### II.A.4. Calibration of the dosimeters

In order to be able to use the EPR dosimeter signal to measure absorbed dose to water during irradiation with the  $^{192}\text{Ir}$  source, the signal per mean absorbed dose in the dosimeter,  $\bar{D}_{\text{det}}$ , needs to be known (see Sec. III A). To achieve this, the dose response of the dosimeters in terms of absorbed dose to water was first determined using a beam quality at which absolute dosimetry is feasible. A subset of the batch (five dosimeters) was thereby irradiated in a clinical 6 MV photon beam in the same PMMA phantom as used in the dose-response homogeneity control (Sec. II A 3) but now at 8.4 cm depth in a  $10 \times 10 \text{ cm}^2$  field at SSD of 100 cm. An ion chamber (Farmer NE 2571), with a  $^{60}\text{Co}$  absorbed dose to water calibration factor traceable to the Swedish Secondary Standards Dosimetry Laboratory, was irradiated simultaneously at the same depth as the dosimeters. The absorbed dose to water was estimated following the IAEA protocol<sup>26</sup> using beam quality correction factors valid for the 6 MV photon beam under reference conditions in a water phantom ( $10 \times 10 \text{ cm}^2$  field, SSD of 100 cm, and 10 cm depth).

The irradiation setup used here closely matches that recommended for absolute dosimetry using plastic phantoms.<sup>27</sup> From Seuntjens *et al.*,<sup>27</sup> it is clear that the nonreference conditions obtained by using a PMMA phantom instead of the

reference water phantom introduces a small error in perturbation correction factors (see Table III in the cited reference) which is accounted for in the uncertainty analysis (Sec. III C 1). The homogeneity of the beam for the  $10 \times 10 \text{ cm}^2$  field at the calibration depth was determined using diodes to be within 0.3%.

The calibration curve is described by

$$I_w = a \cdot D + b, \quad (1)$$

where  $I_w$  is the signal ( $\text{mg}^{-1}$ ),  $a$  ( $\text{mg}^{-1}\text{Gy}^{-1}$ ) the slope of the curve,  $b$  its intercept with the signal axis, and  $D$  the absorbed dose to water. Since all dosimeters of a batch already had obtained a dose (in the dose-response homogeneity control, Sec. II A 3) and since the corresponding signal is not erased during readout, the intercept with the signal axis will be non-zero. The calibration curve is determined by using a subset of five dosimeters as reference dosimeters, whose signals represent the background signal of the batch. The parameters of the calibration curve were calculated using the weighted least-squares matrix method<sup>28</sup> by fitting a straight line to the (dose, signal) points given by the two sets of reference dosimeters. Since all dosimeters of a batch have been shown to have the same dose response in the homogeneity control (Sec. II A 3), the resulting curve is taken to be representative for the whole batch. To avoid differences in signal fading, humidity, etc., all dosimeters of a batch are read out during one and the same day. As recommended by Nagy,<sup>29</sup> the dose administered to the ion chamber calibrated dosimeters was chosen to encompass the dose range given with the  $^{192}\text{Ir}$  source. The time gap between ion chamber calibration and  $^{192}\text{Ir}$  irradiation was 1–3 days. The storage time between irradiation and EPR read out was well within the 28 days for which no signal fading has been observed.<sup>19</sup> Thus, potential, as yet undetected, signal fading would not introduce additional uncertainties in a time span relevant for clinical dosimetry.

## II.B. Experimental setup for measurements in the $^{192}\text{Ir}$ beam

The PMMA phantom used consisted of eight rectangular slabs (with a cross-sectional area  $20 \times 20 \text{ cm}^2$  to a total height of 18 cm) with a central hole to accommodate a catheter with the  $^{192}\text{Ir}$  source (Fig. 2, left). Slab number 5 contained 12 extra holes to house dosimeters (Fig. 2, right). The centers of the dosimeters were thus 8.75 cm from the phantom bottom. Dosimeters were positioned 1, 3, and 5 cm perpendicularly out from the central hole (see Fig. 2). To minimize effects of an eventual deviation of the source position from the center in the catheter during the irradiation, the mean value of the readings of the four dosimeters at each distance was used.

Three experiments were conducted. The first was performed with a GammaMed Plus HDR source model, the second was a repetition of the first using the same afterloading unit but performed after a source exchange and thus for another source, while the third was carried out with a microSelectron-v1 PDR source.

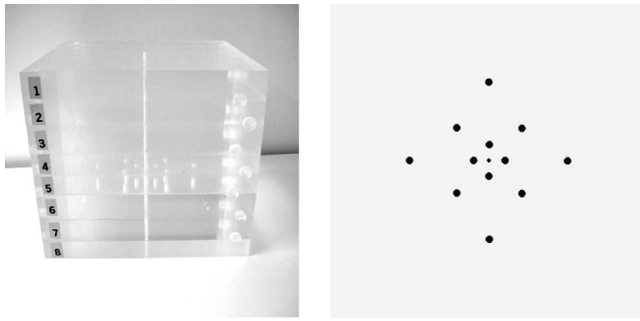


FIG. 2. The PMMA phantom used in the measurements with the  $^{192}\text{Ir}$  source consists of eight slabs forming a rectangular phantom of dimensions  $18 \times 20 \times 20 \text{ cm}^3$ . In slab number 5 inserts for dosimeters were drilled at 1, 3, and 5 cm from the center of the hole through which the  $^{192}\text{Ir}$  source can pass. The positions (top view) of the dosimeters in the slabs are shown to the right.

To reduce the steepness of the dose gradients in the radial and longitudinal directions, a linear irradiation pattern accomplished by stepping the source was used. The source was stepped over a total length of 7 cm obtained in 0.5 cm steps, with the dwelling time at each position optimized (by the TPSs) to produce an as homogeneous dose distribution as possible in the longitudinal direction (coinciding with the direction of the  $^{192}\text{Ir}$  source channel and the axial direction of the dosimeters). In the two HDR experiments, all dosimeters were irradiated in one run, resulting in different absorbed doses to the dosimeters depending on distance from the source. The PDR experiment was designed to give approximately the same dose to the dosimeters at all distances. Irradiation was therefore performed in three consecutive runs, in the intervals between which the inner dosimeters (first those at 1 cm and thereafter those at 3 cm) were removed from the phantom and replaced by lithium formate dummies.

For later comparisons with the experimental results, values of absorbed dose to water at 1, 3, and 5 cm were calculated using the Brachyvision (Varian Medical Systems Inc., Palo Alto, CA) TPS for the HDR experiments and with the Plato TPS (Nucletron BV, Veenendaal, The Netherlands) for the PDR experiment. The values obtained using these planning systems are based on precalculated single-source data, originally derived by Monte Carlo simulations in a cylindrical water phantom of diameter and height 40 cm in the case of the GammaMed Plus HDR source<sup>30</sup> and in a spherical water phantom of radius 15 cm in the case of the microSelectron-v1 PDR source.<sup>31</sup>

### III. CALCULATIONS TO CONVERT MEASURED SIGNALS IN THE Ir BEAM TO ABSORBED DOSE TO WATER IN WATER PHANTOMS USED BY TPS

In Sec. III A, we describe the theory leading to an expression [Eq. (10)] used to convert measured signals to absorbed dose to water in a water phantom of the size and shape used

by the TPS. In Sec. III B, we derive values for the conversion and correction factors defined in Sec. III A. In Sec. III C, an uncertainty budget is made.

#### III.A. Theory

The signal  $M$  per unit absorbed dose in the dosimeter,  $\bar{D}_{\text{det}}$ , can be derived from the absorbed dose to water calibration in the 6 MV photon beam using the identity

$$\frac{M}{\bar{D}_{\text{det}}} = \frac{M}{D_w} \cdot \frac{D_w}{\bar{D}_{\text{det}}} \quad (2)$$

Here,  $M$  denotes the net signal  $l_w - b$  (see Sec. II A 4) and  $D_w$  the absorbed dose to water at the position of the detector (dosimeter) at calibration. With the assumption that the signal per unit absorbed dose in the detector is the same independent of beam quality, i.e., that

$$\left[ \frac{M}{\bar{D}_{\text{det}}} \right]_{\text{Ir}} = \left[ \frac{M}{\bar{D}_{\text{det}}} \right]_{6 \text{ MV}} \quad (3)$$

the absorbed dose to water at a point  $r$  in the PMMA phantom,  $D_{w,\text{phan}}(r)$ , when irradiated in the Ir beam can be determined from

$$[D_{w,\text{phan}}(r)]_{\text{Ir}} = M_{\text{Ir}} \cdot \left[ \frac{M}{\bar{D}_{\text{det}}} \right]_{\text{Ir}}^{-1} \cdot \left[ \frac{D_{w,\text{phan}}(r)}{\bar{D}_{\text{det}}} \right]_{\text{Ir}} \quad (4)$$

If the dosimeter is positioned with its center at  $r$ , the last factor on the right hand side of Eq. (4) can be evaluated from

$$\begin{aligned} \frac{D_{w,\text{phan}}(r)}{\bar{D}_{\text{det}}} &= \frac{\int_0^{h\nu_{\text{max}}} \left[ \frac{\mu_{\text{en}}(h\nu, r)}{\rho} \right]_w \cdot \Psi(h\nu, r)_{\text{phan}} \cdot d(h\nu)}{\int_0^{h\nu_{\text{max}}} \left[ \frac{\mu_{\text{en}}(h\nu, r)}{\rho} \right]_{\text{det}} \cdot \Psi(h\nu, r)_{\text{phan}} \cdot d(h\nu)} \\ &\quad \cdot \frac{\int_0^{h\nu_{\text{max}}} \left[ \frac{\mu_{\text{en}}(h\nu, r)}{\rho} \right]_{\text{det}} \cdot \Psi(h\nu, r)_{\text{phan}} \cdot d(h\nu)}{\bar{D}_{\text{det}}} \\ &= \left[ \frac{\bar{\mu}_{\text{en}}}{\rho}(r) \right]_{\text{det}}^w \cdot f_{\text{vol}}(r). \end{aligned} \quad (5)$$

Here,  $\Psi(h\nu, r)_{\text{phan}} \cdot d(h\nu)$  is the energy fluence of photons with energies in the interval  $h\nu, h\nu + d(h\nu)$  at point  $r$  in the undisturbed phantom,  $[(\mu_{\text{en}}/\rho)(h\nu, r)]_i$  the corresponding mass-energy absorption coefficients for  $i = \text{water}$  and detector material,  $[(\bar{\mu}_{\text{en}}/\rho)(r)]_{\text{det}}^w$  the quotient of an energy fluence weighted average of the mass-energy absorption coefficients for the energy spectrum at  $r$ , and  $f_{\text{vol}}(r)$  a correction factor for volume averaging taking into account the finite size of the detector. From Eq. (5),  $f_{\text{vol}}(r)$  is defined by

$$f_{\text{vol}}(r) = \frac{\int_0^{h\nu_{\text{max}}} \left[ \frac{\mu_{\text{en}}(h\nu, r)}{\rho} \right]_{\text{det}} \cdot \Psi(h\nu, r)_{\text{phan}} \cdot d(h\nu)}{\bar{D}_{\text{det}}}. \quad (6)$$

In measurements with an Ir source, the detector approximates one in which charged particle equilibrium (CPE) is established. Hence, the absorbed dose equals the collision kerma for the detector material, a fact utilized in deriving Eq. (5) above. In the calibration with 6 MV roentgen radiation, CPE does not exist in the detector. The Burlin theory can be applied to derive  $\bar{D}_{\text{det}}$  for use in calculating the value of  $M/\bar{D}_{\text{det}}$ .

Since the dosimeters were positioned in a PMMA phantom when irradiated in the 6 MV calibration beam, the Burlin cavity theory conversion coefficient  $\bar{f}_B = \bar{D}_{\text{det}}/D_{\text{med}}$  has to be evaluated with PMMA as the medium surrounding the detector. The calibration with the ion chamber gives the absorbed dose to water in a small Bragg-Gray cavity in the PMMA phantom. This can be converted to absorbed dose to PMMA by multiplying the calibration coefficient with the mass collision stopping power ratio PMMA/water,  $(\bar{m}\bar{s}_{\text{col}})_{\text{w}}^{\text{PMMA}}$ . We then have

$$\left[ \frac{M}{\bar{D}_{\text{det}}} \right]_{6 \text{ MV}} = \left[ \frac{M}{D_{\text{w}}} \right]_{6 \text{ MV}} \cdot [(\bar{m}\bar{s}_{\text{col}})_{\text{w}}^{\text{PMMA}} \cdot \bar{f}_B]_{6 \text{ MV}}^{-1}. \quad (7)$$

Finally, combining Eqs. (3), (4), (5), and (7) we get

$$[D_{\text{w,phan}}(r)]_{\text{Ir}} = M_{\text{Ir}} \cdot \left[ \frac{D_{\text{w}}}{M} \cdot [(\bar{m}\bar{s}_{\text{col}})_{\text{w}}^{\text{PMMA}} \cdot \bar{f}_B]_{6 \text{ MV}} \right] \cdot \left[ \left[ \frac{\bar{\mu}_{\text{en}}(r)}{\rho} \right]_{\text{det}}^{\text{w}} \cdot f_{\text{vol}}(r) \right]_{\text{Ir}}, \quad (8)$$

where  $D_{\text{w}}/M$  is given by the inverse  $1/a$  of the slope  $a$  of the calibration curve [Eq. (1)].

In our experiments, the points  $r$  are defined by the radial distance  $r$  from the center of the phantom (see Fig. 2). In order to compare the measured absorbed doses as determined using Eq. (8) with those derived by the TPS, two further corrections have to be applied. These are as follows

- (1) A correction to account for possible deviations of the source position from the center of the phantom during the irradiation has to be applied. It was assumed that this could be achieved by taking the mean  $\bar{M}_{\text{Ir}}(r)$  of the signals of four dosimeters positioned at equal distance around the center of the phantom (see Fig. 2).
- (2) The absorbed dose to water in the PMMA phantom,  $D_{\text{w,phan}}(r)$ , has to be converted to absorbed dose to water in a water phantom  $D_{\text{w,w}}(r)$  of the same size and shape as those used by the TPS.

The absorbed dose to water,  $D_{\text{w,w}}(r)$ , which is to be compared to the absorbed dose to water calculated by the TPS, is then obtained from

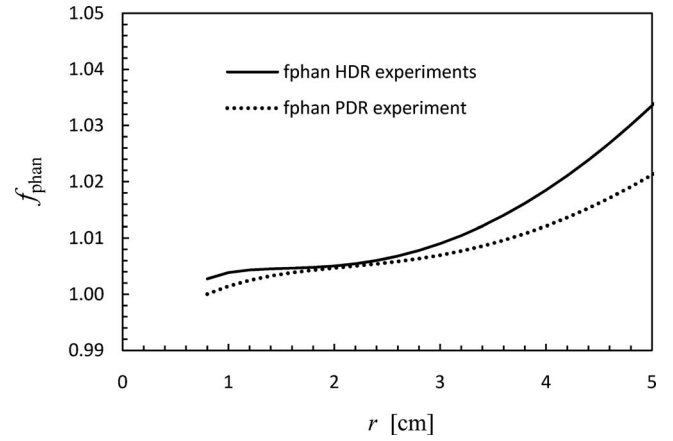


FIG. 3. The phantom correction factors  $f_{\text{phan}}$  as a function of distance to phantom center,  $r$ , to correct for using an experimental phantom of different medium (PMMA) and size than the reference water phantoms underlying dose calculations of the treatment planning system used with the GammaMed Plus HDR source and the microSelectron-v1 PDR source.

$$D_{\text{w,w}}(r) = \bar{D}_{\text{w,phan}}(r) \cdot \frac{D_{\text{w,phan}}(r)}{\bar{D}_{\text{w,phan}}(r)} \cdot f_{\text{phan}}(r). \quad (9)$$

Here  $D_{\text{w,phan}}(r)$  is the absorbed dose to water in the PMMA phantom when the source is correctly positioned with its center at the center of the phantom and  $\bar{D}_{\text{w,phan}}(r)$  the absorbed dose derived from Eq. (8) using the mean  $\bar{M}_{\text{Ir}}(r)$  of the signals from four dosimeters. It is assumed that the factor  $D_{\text{w,phan}}(r)/\bar{D}_{\text{w,phan}}(r)$  equals 1, i.e., that by taking the mean of the four dosimeter signals, the correct value for  $D_{\text{w,phan}}(r)$  is obtained. The uncertainty introduced by this assumption is estimated in the uncertainty analysis [see Eq. (19) in Sec. III C 1]. The factor  $f_{\text{phan}}(r)$  converts absorbed dose to water measured in the experimental phantom,  $D_{\text{w,phan}}(r)$ , to absorbed dose to water in a water phantom of the size and shape used by the TPS,  $D_{\text{w,w}}(r)$ , and is given by

$$f_{\text{phan}}(r) = D_{\text{w,w}}(r)/D_{\text{w,phan}}(r). \quad (10)$$

The absorbed dose to water,  $D_{\text{w,w}}(r)$ , in a water phantom of the size and shape used by the TPS is finally obtained from [with  $D_{\text{w,phan}}(r)/\bar{D}_{\text{w,phan}}(r)=1$  as discussed above]

$$[D_{\text{w,w}}(r)]_{\text{Ir}} = \bar{M}_{\text{Ir}} \cdot \left[ \frac{D_{\text{w}}}{M} \cdot [(\bar{m}\bar{s}_{\text{col}})_{\text{w}}^{\text{PMMA}} \cdot \bar{f}_B]_{6 \text{ MV}} \right] \cdot \left[ \left[ \frac{\bar{\mu}_{\text{en}}(r)}{\rho} \right]_{\text{det}}^{\text{w}} \cdot f_{\text{vol}}(r) \cdot f_{\text{phan}}(r) \right]_{\text{Ir}}. \quad (11)$$

Values for the conversion and correction factors were calculated for  $r=1, 3$ , and  $5$  cm as described below.

### III.B. Calculation of correction and conversion factors

#### III.B.1. Burlin cavity theory conversion factor

##### $\bar{f}_B$

The Burlin theory treats the case of a detector positioned with its center at a point  $P$  inside an irradiated medium in

which CPE exists at  $P$  when the dosimeter is not present. For monoenergetic photons, the relation  $f_B = \bar{D}_{\text{det}}/D_{\text{med}}(P)$  is given by<sup>32</sup>

$$f_B = \frac{\bar{D}_{\text{det}}}{D_{\text{med}}(P)} = d \cdot [\bar{\mu}_{\text{col}}]_{\text{med}}^{\text{det}} + (1-d) \cdot \left[ \frac{\mu_{\text{en}}}{\rho} \right]_{\text{med}}^{\text{det}}. \quad (12)$$

The weighting factor  $d$  is given by  $d = (1 - e^{-\beta \cdot g}) / \beta \cdot g$ , where  $g$  is the mean chord length in the detector. Here,  $d$  was calculated using  $g = 4 \cdot V/S$  with  $V$  the detector volume,  $S$  its surface area, and  $\beta = 16.0 / (E_{\text{max}} - 0.036)^{1.40}$  cm<sup>2</sup>/g where  $E_{\text{max}}$  is the maximum energy of the secondary electrons released by the photons (expressed in MeV). The maximum energy of the Compton electrons released was used for  $E_{\text{max}}$ . A small deviation from ideal CPE conditions at 6 MV will affect the values of the nominator and denominator in Eq. (12) to the same degree of accuracy and is hence neglected in the following.

Both the weighting factor  $d$  and the quotient of the mass-energy absorption coefficients depend on photon energy. The conversion factor  $\bar{f}_B$  averaged over the photon energy spectrum is obtained from

$$\begin{aligned} \bar{f}_B(P) &= \frac{\int_0^{h\nu_{\text{max}}} f_B(h\nu, P) \cdot D_{\text{med}}(h\nu, P) \cdot d(h\nu)}{D_{\text{med}}(P)} \\ &= \int_0^{h\nu_{\text{max}}} f_B(h\nu, P) \cdot \frac{D(h\nu, P)_{\text{med}}}{D(P)_{\text{med}}} \cdot d(h\nu). \end{aligned} \quad (13)$$

Here,

$$D(h\nu, P)_{\text{med}} = \left[ \frac{\mu_{\text{en}}}{\rho}(h\nu, P) \right]_{\text{med}} \cdot \Psi(h\nu, P)_{\text{med}}, \quad (14)$$

where  $\Psi(h\nu, P)_{\text{med}} \cdot d(h\nu)$  is the energy fluence of photons with energies in the interval  $h\nu, h\nu + d(h\nu)$  at point  $P$  in the medium and  $D_{\text{med}}(P) = \int D(h\nu, P)_{\text{med}} \cdot d(h\nu)$ .

The conversion coefficient  $\bar{f}_B$  was calculated using photon and electron energy spectra simulated with the EGSnrc (Ref. 33) user code FLURZnrc (Ref. 34) to calculate appropriately averaged values of the ratios of mass collision stopping powers,  $[\bar{\mu}_{\text{col}}]_{\text{PMMA}}^{\text{lithium formate}}$ , and mass-energy absorption coefficients,  $[\bar{\mu}_{\text{en}}/\rho]_{\text{PMMA}}^{\text{lithium formate}}$ . In the simulations, a circular photon beam of diameter of 10 cm was incident on a PMMA phantom of similar size (diameter of 20 cm and height of 14 cm) to that used in the calibration (Sec. II A 4) and energy spectra at 8.4 cm depth (SSD of 100 cm) were derived. The incident beam was simulated using a 6 MV accelerator spectrum from Mohan *et al.*,<sup>35</sup> supplied with the EGSnrc distribution. Values of mass stopping powers and mass-energy absorption coefficients were taken from NIST.<sup>36,37</sup> A value of the factor  $(\bar{\mu}_{\text{col}})_w^{\text{PMMA}}$  in Eqs. (7) and (8) was calculated using the same Monte Carlo simulated electron energy spectrum as in calculating  $[\bar{\mu}_{\text{col}}]_{\text{PMMA}}^{\text{lithium formate}}$ . The numerical value of  $(\bar{\mu}_{\text{col}})_w^{\text{PMMA}} \cdot \bar{f}_B$  was determined to be 0.9240.

### III.B.2. Conversion factor $[\bar{\mu}_{\text{en}}/\rho]_{\text{det}}^w$ and correction factor $f_{\text{phan}}$

The factors  $[\bar{\mu}_{\text{en}}/\rho]_{\text{det}}^w$  of Eqs. (5) and (8) and  $f_{\text{phan}}$  defined in Eq. (10) and used in Eq. (11) were obtained as described below based on results of EGSnrc Monte Carlo simulations to derive photon energy fluence spectra and values of absorbed dose with the usercodes FLURZnrc (Ref. 34) and DOSRZnrc.<sup>34</sup> A cylindrical PMMA phantom of diameter and height 20 cm represented the experimental phantom, a cylindrical water phantom of diameter and height 40 cm the doses used in TPS data for the HDR source, and a cylindrical water phantom of diameter and height 30 cm the doses used in TPS data for the PDR source. The Monte Carlo settings were the same as in the paper (this issue) by Carlsson Tedgren and Alm Carlsson.<sup>38</sup> However, for this work, simulations of the  $^{192}\text{Ir}$  point source emitting a photon energy spectrum for a typical, steel-encapsulated  $^{192}\text{Ir}$  source<sup>39</sup> were performed not only with the source centrally positioned in the phantoms but also with it displaced from the center, along both the axial directions, by 0.5, 1.0, 1.5, 2.0, 2.5, 3.0, and 3.5 cm to represent the dwelling positions. Dose values and spectra were still scored along the central radius of the phantom (corresponding to the detector positions). Spectra and values of absorbed doses representing the actual dwelling time sequences were derived by adding the spectra and doses for the individual dwelling positions weighted by the dwelling time in each position.

Values of  $[\bar{\mu}_{\text{en}}/\rho]_{\text{lithium formate}}^w$  were determined by averaging, over the energy fluence spectrum in the experimental phantom, water and lithium formate mass-energy absorption coefficients using data from NIST.<sup>36</sup> The values of  $[\bar{\mu}_{\text{en}}/\rho]_{\text{lithium formate}}^w$  were 1.0807, 1.0820, and 1.0834 at 1, 3, and 5 cm, respectively.

Values of the phantom correction factor  $f_{\text{phan}}$ , defined in Eq. (10), are shown in Fig. 3. Values used to correct the HDR measurements were 1.004, 1.009, and 1.034 at 1, 3, and 5 cm from the source. The corresponding values for the PDR measurements were 1.001, 1.007, and 1.021. Different correction factors are obtained due to the different sizes and shapes of the water phantoms underlying the reference data used in the TPS systems Brachyvision by Varian (a cylinder of diameter and height 40 cm)<sup>30</sup> and Plato by Nucletron (a sphere of diameter 30 cm).<sup>31</sup> Differences between phantoms of cubic and cylindrical shape are small, while they are larger for spherical phantoms.<sup>40</sup> Based on the results from Granero *et al.*,<sup>40</sup> an additional small correction to account for the spherical shape of the water phantom underlying the Nucletron TPS data in relation to the values obtained by us in simulating cylindrical phantoms was introduced for the value of  $f_{\text{phan}}$  at 5 cm.

### III.B.3. Volume averaging correction factor $f_{\text{vol}}$

The volume averaging correction factor  $f_{\text{vol}}$  defined in Eq. (6) was calculated using known values of absorbed dose to water as a function of position as obtained from the TPS. A detailed description follows.

Consider cylindrical coordinate systems  $S(O, r, \varphi, z)$  and  $S'(O', r', \varphi', z')$ , see Fig. 4. The axes  $z$  and  $z'$  coincide with the source positions and the cylindrical detector axis, respectively, and are parallel to each other. The Cartesian axis  $x'$  is rotated so that it intersects the origin  $O$  of coordinate system  $S$ .

The coordinates  $(r, \varphi, z)$  of a point  $P$  in  $S$  are expressed via coordinates  $(r', \varphi', z')$  in  $S'$  as

$$r = r(r', \varphi') = (d^2 + r'^2 + 2dr' \cos \varphi')^{1/2}, \tag{15}$$

$$\varphi = \varphi(r', \varphi'), \tag{16}$$

$$z = z(z') = h + z'. \tag{17}$$

Equation (15) follows from the cosine formula for the triangle  $OO'P$  where  $\cos \alpha = \cos(\pi - \varphi') = -\cos \varphi'$ . The explicit form of Eq. (16) will not be needed and Eq. (17) follows from Fig. 4(b). The volume averaging correction factor was calculated in the cylindrical coordinates of system  $S'$  as

$$\begin{aligned} f_{\text{vol}} &= \left[ V^{-1} \int_{V_{\text{det}}} D_{\text{det,phan}}(\mathbf{r}) / K_{c,\text{det,phan}}(O') dV \right]^{-1} \\ &= \left[ V^{-1} \int_{V_{\text{det}}} q(\mathbf{r}) dV \right]^{-1} \\ &= \left[ V^{-1} \int_{-H/2}^{H/2} \int_0^{2\pi} \int_0^R q(r(r', \varphi'), \varphi(r', \varphi'), z(z')) r' dz' d\varphi' dr' \right]^{-1} \\ &= \left[ V^{-1} \int_{-H/2}^{H/2} \int_0^{2\pi} \int_0^R q'(\sqrt{d^2 + r'^2 + 2dr' \cos \varphi'}, h + z') r' dz' d\varphi' dr' \right]^{-1}, \end{aligned} \tag{18}$$

where  $V = \pi R^2 H$  is the volume of the cylindrical detector of height  $H$  and radius  $R$  and  $q(\mathbf{r}) = D(\mathbf{r})_{\text{det,phan}} / K_{c,\text{det,phan}}(O')$  gives the absorbed dose to the detector in the water phantom at a point  $r$  relative to the lithium formate collision kerma in the water phantom at the center of the detector. It was assumed that (i) the condition of CPE was fulfilled, and thus  $K_{c,\text{det,phan}}(O') = D(O')_{\text{det,phan}}$ , and (ii) the setup was axially symmetric and thus the function  $q'(r, z) = q(r, \varphi, z)$  did not depend on  $\varphi'$ . The right hand side of Eq. (18) was calculated numerically using the adaptive integration method<sup>41</sup> available in the object oriented data analysis framework ROOT.<sup>42</sup>

For a given point  $r$ , cubic splines and linear interpolations in the radial and axial directions, respectively, were used to determine the value of  $q(r, z)$  from a grid of known values. An example of the dose profiles is shown in Fig. 5(a). The resulting  $f_{\text{vol}}$  as a function of position is given in Fig. 5(b). At distances of 1, 3, and 5 cm, the values were 0.9932, 0.9992, and 0.9998. Estimates to translate the results to the case with measurements within the PMMA phantom indicate that the correction factors derived using the water phantom data will not significantly change values of  $f_{\text{vol}}$ .

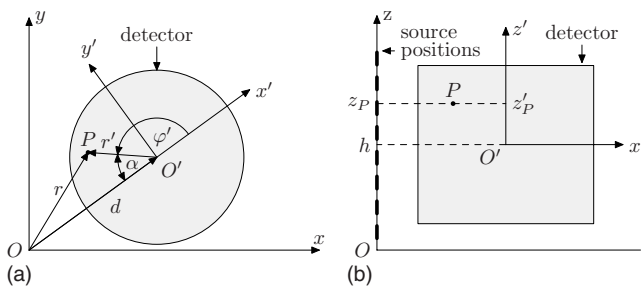


FIG. 4. Schematic (a) top and (b) side views of cylindrical coordinate systems  $S(O, r, \varphi, z)$  and  $S'(O', r', \varphi', z')$ . The origin  $O'$  of  $S'$  is shifted by distances of  $d$  and  $h$  in the radial and axial directions, respectively. Radii  $r$  and  $r'$  give the distances from the corresponding  $z$  axes. Angles  $\varphi$  and  $\varphi'$  are measured from Cartesian coordinate axes  $x$  and  $x'$ , respectively.

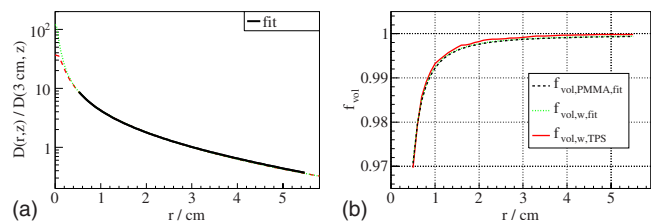


FIG. 5. (a) Normalized profiles of absorbed dose to water in water for depths representing the range of measured values in the dosimeter. The normalized profiles were fitted with the curve  $f(r) = A \exp(-a_w \cdot r) / r$ , where  $A = 4.95 \pm 0.24$  and  $a_w = (0.1632 \pm 0.0038) \text{ cm}^{-1}$ . (b) The volume correction factor  $f_{\text{vol}}$  as a function of radial distance  $r$  for the measured dose profiles (full line) and the fitted curve  $f$  (dotted). The black dotted line shows values representative for PMMA.

### III.C. Uncertainty budget

The uncertainties were evaluated following the “Guide to the Expression of Uncertainties in Measurements” (GUM) published by the IOS.<sup>43</sup>

#### III.C.1. Uncertainty in the experimentally determined absorbed dose

The combined relative standard uncertainty in absorbed dose,  $u(D_{w,w}(r))/D_{w,w}(r)$ , derived from the measurements using Eq. (11), was estimated by adding the uncertainties of its parameters according to the law of propagation of uncertainty. Neglecting any possible correlations between the factors in Eq. (11), we have

$$\begin{aligned} \left[ \frac{u(D_{w,w}(r))}{D_{w,w}(r)} \right]^2 &= \left[ \frac{u(\bar{M}_{\text{Ir}})}{M_{\text{Ir}}} \right]^2 + \left[ \frac{u\left(\frac{D_w}{M}\right)}{\frac{D_w}{M}} \right]^2 \\ &+ \left[ \frac{u\left(\frac{(\bar{m}\bar{s}_{\text{col}})_{\text{w}}^{\text{PMMA}}}{(\bar{m}\bar{s}_{\text{col}})_{\text{w}}^{\text{PMMA}}}\right)}{\frac{(\bar{m}\bar{s}_{\text{col}})_{\text{w}}^{\text{PMMA}}}{(\bar{m}\bar{s}_{\text{col}})_{\text{w}}^{\text{PMMA}}}} \right]^2 + \left[ \frac{u(\bar{f}_B)}{\bar{f}_B} \right]^2 \\ &+ \left[ \frac{u\left(\left[\frac{\bar{\mu}_{\text{en}}}{\rho}\right]_{\text{det}}^{\text{w}}\right)}{\left[\frac{\bar{\mu}_{\text{en}}}{\rho}\right]_{\text{det}}^{\text{w}}} \right]^2 + \left[ \frac{u(f_{\text{vol}})}{f_{\text{vol}}} \right]^2 \\ &+ \left[ \frac{u(f_{\text{phan}})}{f_{\text{phan}}} \right]^2 + \left[ \frac{u\left(\frac{D_{w,\text{phan}}}{\bar{D}_{w,\text{phan}}}\right)}{\frac{D_{w,\text{phan}}}{\bar{D}_{w,\text{phan}}}} \right]^2. \quad (19) \end{aligned}$$

Below follows an estimation of the relative standard uncertainty (standard deviation) for each of the factors in Eq. (19). Numerical values are reported in Table III (Sec. IV).

The uncertainty in a single dosimeter signal  $M_{\text{Ir}}=l_w-b$  depends on the uncertainties in both the signal  $l_w$  and the background signal  $b$ . Type B uncertainties are regarded as negligible, since systematic errors were minimized in the experimental design. Efforts to reduce systematic errors include weighing of dosimeters before and after readout, spreading out the five readouts of one dosimeter during the day, storing all dosimeters under the same environmental conditions, and so on (Sec. II A 3). The uncertainty in the signal  $l_w$  was taken to be the value of 0.6% (the standard deviation determined from the readings in the homogeneity test). The relative standard deviation in  $b$  is determined by the same figure; however, since  $b$  is given by the average signal of five dosimeters its uncertainty is further divided by  $\sqrt{5}$ .

The relative uncertainty in the inverse of the dose response  $u(D_w/M)/(D_w/M)$  is equal to the relative uncertainty in  $a$ , which is given by the least-squares fit. It depends on the uncertainties in the absorbed doses and the corresponding signals of the points determining the calibration curve. To take into account the uncertainty for use of the ion chamber outside full reference conditions,<sup>27</sup> the uncertainty in the ab-

sorbed dose to water at calibration is estimated to be 1.1%, a figure that is slightly higher than the value of 0.8% estimated for the determination of absorbed dose to water at hospitals in the IAEA protocol.<sup>26</sup> The contribution of the covariance between  $a$  and  $b$  to the total combined relative uncertainty was found to be negligible (around 1% of that in the signal), similar to findings reported for an EPR/alanine system by Anton.<sup>44</sup>

Values of the quotients of mass-energy absorption coefficients  $[(\bar{\mu}_{\text{en}}/\rho)_{\text{lithium formate}}^{\text{w}}]$  and mass collision stopping powers  $[(\bar{m}\bar{s}_{\text{col}})_{\text{w}}^{\text{PMMA}}]$  at 6 MV and in the phantom correction factor  $f_{\text{phan}}$  are all derived using energy spectra and dose values derived in actual phantoms from Monte Carlo simulations. The uncertainties in these quantities are hence low and the relative standard deviation (type B estimation) is estimated to be 0.5%. The uncertainty in  $f_{\text{phan}}$  at 5 cm is increased to 0.7% since corrections for phantom size and shape increase with increasing distance from the source.<sup>38,40</sup>

The uncertainty in the Burlin conversion coefficient  $\bar{f}_B$  is estimated by assuming a maximum deviation  $\bar{f}_{B,\text{max}}-\bar{f}_{B,\text{min}}$  as caused by assuming the weighting factors to be  $d=1$  (the detector is a small Bragg-Gray detector) and  $d=0$  (the detector is a “large” detector in which CPE prevails) at all photon energies. A triangular distribution is assumed for the type B estimation of the standard deviation.

The uncertainty in correction factor  $D_{w,\text{phan}}(r)/\bar{D}_{w,\text{phan}}(r)$  is estimated by assuming the source dwell positions to be misaligned into positions at most 0.5 mm away from the center of the 3 mm diameter hole for the catheter and comparing the mean of the absorbed doses at the positions of the four dosimeters with the value obtained with correctly positioned source steps. The relative standard uncertainty (type A) was estimated using Monte Carlo simulation assuming a constant probability for the source to take any position within a circle of radius of 0.5 mm around the center of the phantom.

The uncertainty in the volume averaging correction factor  $f_{\text{vol}}$  is estimated by studying the influence of the uncertainty in positioning ( $\pm 0.5$  mm) of the dosimeters on this factor. The type B estimate of the standard uncertainty is derived assuming a rectangular distribution.

#### III.C.2. Uncertainty in the absorbed dose calculated by the TPS

The total combined relative standard uncertainty in the absorbed dose given by the TPS is estimated from

$$\left[ \frac{u(D_{w,\text{TPS}})}{D_{w,\text{TPS}}} \right]^2 = \left[ \frac{u(D_{w,\text{MC}})}{D_{w,\text{MC}}} \right]^2 + \left[ \frac{u(\text{RAKR})}{\text{RAKR}} \right]^2, \quad (20)$$

where  $u(D_{w,\text{MC}})$  is the uncertainty in the Monte Carlo simulation data from which the TPS dose values are derived and  $u(\text{RAKR})$  the uncertainty in the reference air kerma rate. The source certificate states that the expanded (coverage factor of 3) combined standard uncertainty in source calibration is  $\pm 5\%$  of the reference air kerma rate, which gives a relative standard deviation of approximately 1.7%.

TABLE I. Measured absorbed doses  $[D_{w,w}(r)]_{\text{Ir}}$ , absorbed doses given by the treatment planning system,  $[D_{w,\text{TPS}}(r)]_{\text{Ir}}$ , and relative deviation  $(D_{w,w}(r) - D_{w,\text{TPS}}(r)) / D_{w,\text{TPS}}(r)$  for the two HDR experiments. Uncertainties in the absorbed doses  $D_{w,\text{TPS}}$  and  $D_{w,w}$  are given in terms of expanded (coverage factor of 2) combined standard uncertainties (see Table III) corresponding to 95% confidence intervals.

$r$ (cm)	Measurement 1			Measurement 2	
	$[D_{w,\text{TPS}}(r)]_{\text{Ir}}$ (Gy)	$[D_{w,w}(r)]_{\text{Ir}}$ (Gy)	Relative deviation (%)	$[D_{w,w}(r)]_{\text{Ir}}$ (Gy)	Relative deviation (%)
1	$25.39 \pm 1.62$	$25.28 \pm 0.66$	-0.4	$25.33 \pm 0.66$	-0.2
3	$6.04 \pm 0.39$	$5.94 \pm 0.17$	-1.5	$6.01 \pm 0.17$	-0.4
5	$2.57 \pm 0.17$	$2.50 \pm 0.09$	-2.9	$2.54 \pm 0.09$	-1.3

Granero *et al.*<sup>45</sup> evaluated the dose rate uncertainty for an  $^{192}\text{Ir}$  source similar to the one used in this work following the recommendation of the TG-43U1 report<sup>3</sup> and including both type A and type B uncertainties. The combined relative standard deviation of 2.7% obtained by these authors is used here as an estimate of  $u(D_{w,\text{MC}}(r)) / D_{w,\text{MC}}(r)$ .

#### IV. RESULTS

The absorbed doses to water at distance  $r$  from the center of the  $^{192}\text{Ir}$  source,  $D_{w,w}(r)$ , obtained from the experiments and  $D_{w,\text{TPS}}(r)$ , given by the TPS, are listed in Table I for the two experiments with the HDR source model and in Table II for the experiment with the PDR source model. The relative deviation defined as  $(D_{w,w}(r) - D_{w,\text{TPS}}(r)) / D_{w,\text{TPS}}(r)$  is also given. The combined relative standard uncertainty in  $D_{w,w}(r)$  and  $D_{w,\text{TPS}}(r)$  and their components are given in Table III. In Tables I and II expanded (coverage factor of 2) combined relative uncertainties representing 95% confidence intervals are indicated. These can be considered as the error limits.

The uncertainty in the measured signals  $M_{\text{Ir}}$  depends on the background absorbed dose (from the homogeneity test) and the absorbed doses registered by the dosimeters at irradiation in the PMMA phantom. The two values given in Table III are the uncertainties in the HDR and PDR (HDR/PDR) experiments, respectively. The corresponding background absorbed doses were 3 Gy/7 Gy. In the HDR experiments, all dosimeters were irradiated during the same session with the maximum and minimum registered absorbed doses being 25 Gy (at 1 cm) and 3 Gy (at 5 cm). In the PDR

experiment, three irradiation sessions were used so as to obtain approximately the same absorbed dose in the dosimeters (15 Gy) at all distances.

The results in Tables I and II show that the experimentally determined absorbed doses to water agree well within the estimated uncertainties with the absorbed doses calculated by the TPS. The deviations range from +1.4% to -2.9% and indicate that the uncertainties have not been underestimated in our analysis.

#### V. DISCUSSION

The combined relative standard uncertainty in the experimentally determined absorbed doses is 1.3%–1.7% (see entry 10 in Table III). The largest contribution comes from the spread in the dose response of the dosimeters in any one batch. The correction for the volume averaging effect is small: 0.993 at 1 cm distance and 1.000 at 5 cm from the center. This is because we used a linear pattern for stepping the source to reduce gradients in the radial and longitudinal directions. The dosimeters are larger than the LiF dosimeters normally used to verify single-source dose distributions at short distances. However, in this study, we wanted to test the feasibility of the lithium formate EPR dosimetry system for dose verification. In the next step, we will work on producing EPR dosimeters of smaller size. Using smaller sized dosimeters, the read-out process in the EPR spectrometer needs to be reoptimized. In this work, we used dosimeters for which the optimization procedure has already been worked out and tested.<sup>19,24</sup> Dosimeters of smaller size will be less sensitive and therefore may need higher absorbed doses to reach the same degree of precision. This will not be a problem since the dosimeters have a linear response with respect to absorbed dose over a large dose interval (0.2–1000 Gy).<sup>20</sup> When used to verify absorbed doses from multiple-source implants or stepping sources, they will not meet such steep gradients as those around single sources and hence will be suitable also in their present size. In cases where it is not possible to correct for the variation in photon energy spectrum within the treatment volume, the low-energy dependence will be an advantage. In this study, the weighted mean of the ratio of mass-energy absorption coefficients  $[\bar{\mu}_{\text{en}}/\rho]_{\text{lithium formate}}^w$ , derived using the actual energy fluence spectrum in the PMMA phantom and for the dwelling time sequence used, increased by less than 0.5% between 1 and 5

TABLE II. Measured absorbed doses  $[D_{w,w}(r)]_{\text{Ir}}$ , absorbed doses given by the treatment planning system,  $[D_{w,\text{TPS}}(r)]_{\text{Ir}}$ , and relative deviation  $(D_{w,w}(r) - D_{w,\text{TPS}}(r)) / D_{w,\text{TPS}}(r)$  between the two values for the PDR experiment. Uncertainties in the absorbed doses  $D_{w,\text{TPS}}$  and  $D_{w,w}$  are given in terms of expanded (coverage factor of 2) combined standard uncertainties (see Table III) corresponding to 95% confidence intervals.

$r$ (cm)	Measurement 3		
	$[D_{w,\text{TPS}}(r)]_{\text{Ir}}$ (Gy)	$[D_{w,w}(r)]_{\text{Ir}}$ (Gy)	Relative deviation (%)
1	$15.00 \pm 0.96$	$15.21 \pm 0.43$	+1.4
3	$15.42 \pm 0.99$	$15.51 \pm 0.43$	+0.6
5	$15.71 \pm 1.01$	$15.46 \pm 0.46$	-1.6

TABLE III. Components contributing to the combined relative standard uncertainty in experimentally determined and TPS calculated absorbed doses.

Entry No	Distance from phantom center:	HDR/PDR		
		1 cm	3 cm	5 cm
1	$u(M_{\text{Ir}})/M_{\text{Ir}}$	0.7%/0.9%	1.0%/0.9%	1.3%/0.9%
2	$u(D_w/M)/D_w/M$	0.3%	0.3%	0.3%
3	$u(m_{\text{col}}^{\text{PMMA}}/m_{\text{col}}^{\text{PMMA}})$	0.5%	0.5%	0.5%
4	$u(\bar{f}_B)/\bar{f}_B$	0.5%	0.5%	0.5%
5	$u([\bar{\mu}_{\text{en}}/\rho]_{\text{lithium formate}}^w)/[\bar{\mu}_{\text{en}}/\rho]_{\text{lithium formate}}^w$	0.5%	0.5%	0.5%
6	$u(f_{\text{vol}})/f_{\text{vol}}$	0.2%	0.1%	0.1%
7 (combined 1–6)	$u(D_{w,\text{phan}})/D_{w,\text{phan}}$ [Eq. (8)]	1.2%/1.3%	1.4%/1.3%	1.6%/1.3%
8	$u(f_{\text{phan}})/f_{\text{phan}}$	0.5%	0.5%	0.7%
9	$u(D_{w,\text{phan}}/\bar{D}_{w,\text{phan}})/D_{w,\text{phan}}/\bar{D}_{w,\text{phan}}$	0.05%	0.01%	0.01%
10 (combined 7–9)	$u(D_{w,w})/D_{w,w}$ [Eq. (11)]	1.3%/1.4%	1.4%/1.4%	1.7%/1.5%
11	$u(\text{RAKR})/\text{RAKR}$	1.7%	1.7%	1.7%
12	$u(D_{w,\text{MC}})/D_{w,\text{MC}}$	2.7%	2.7%	2.7%
13 (combined 11–12)	$u(D_{w,\text{TPS}})/D_{w,\text{TPS}}$	3.2%	3.2%	3.2%
14 combined (10+13)	$u(D_{w,w})+u(D_{w,\text{TPS}})/D_{w,w}$	3.4%/3.5%	3.5%/3.5%	3.6%/3.5%

cm from the source at the center of the phantom. The energy spectra used in deriving the  $[\bar{\mu}_{\text{en}}/\rho]_{\text{lithium formate}}^w$  were determined in the current experimental PMMA phantom, which is of comparatively small dimensions. In larger experimental phantoms, there will at the same linear distance from the source be a higher fluence of scattered, energy-degraded photons.<sup>38</sup> This affects the depth dependence of the  $[\bar{\mu}_{\text{en}}/\rho]_{\text{det}}^w$  ratio, accentuating the importance of either performing phantom (and possibly irradiation-pattern) specific corrections or selecting the detector with the lowest energy dependence.

The combined relative standard uncertainty in our experimentally determined absorbed doses is at most 4% (see entry 14 in Table III) and thus lower than the combined relative standard uncertainty in the dose rate constant of 7%–9% stated by TG-43 (Ref. 3) for the LiF TLD single-source dosimetry system. These results are not directly comparable since, in the present work, absorbed dose is not determined for single-source geometry, which is more demanding as regards the dimensions of the dosimeter and positional errors. The data in the TG-43U1 report (Ref. 3) furthermore refer to measurements with low-energy photon-emitting brachytherapy sources for which other types of corrections due to phantom materials, etc., are required. Kirov *et al.*<sup>10</sup> reported combined relative standard uncertainties of 6%–7% when measuring absorbed dose around a single HDR  $^{192}\text{Ir}$  source with LiF TLD at distances of 3–10 cm from the source.

Compared to LiF TL dosimetry, an obvious advantage of the lithium formate dosimetry system is its larger dynamic range in absorbed dose. The LiF dosimeter has an upper dose limit of approximately 1 Gy after which supralinearity becomes a source of uncertainty. Early studies report results of LiF TL measurements around LDR  $^{192}\text{Ir}$  sources<sup>7</sup> while more recent measurements around PDR and HDR sources have been made after the source has decayed to levels below those used clinically.<sup>10</sup> Using a lithium formate dosimetry system, measurements can be made using sources with clinically rel-

evant activities. Another advantage with the large dynamic range in absorbed dose is the possibility to perform experimental verification of calculated doses over large distances in a single irradiation and that any undesired influence from the transit dose<sup>12,15–17</sup> on experiments can be avoided simply by giving high enough doses for the transit dose to become negligible.

The results in Tables I and II show that in all the experiments the largest deviation between experimental and calculated absorbed doses is obtained at 5 cm distance from the source. This may be caused by a larger attenuation in the dosimeters as compared to that in an equal thickness of PMMA. To avoid such an effect, the position of the holes should be changed so that primary photons only pass through one dosimeter on their way through the phantom. This arrangement is usually used in measurements using TL-LiF dosimeters. The difference in density between PMMA ( $\rho = 1.19 \text{ g/cm}^3$ ) and that of the dosimeters ( $\rho = 1.26 \text{ g/cm}^3$ ) is, however, considerably smaller than that between PMMA and LiF ( $\rho = 2.64 \text{ g/cm}^3$ ), causing less problems with inter-shielding effects. Another possible reason for the larger deviation at 5 cm could be that the size and shape of the phantoms in which the phantom correction factors  $f_{\text{phan}}$  were derived did not exactly match the actual ones. Differences between differently sized phantoms increase with increasing distance from the source.<sup>38</sup>

## VI. CONCLUSIONS

The lithium formate EPR dosimetry system investigated has shown to yield accurate results when used to determine absorbed doses around  $^{192}\text{Ir}$  brachytherapy sources. Its low-energy dependence relative to water makes it more suitable for dose verification than LiF TL dosimetry systems in clinically relevant situations (multisource implants and stepping-source irradiations where the photon energy spectrum in the general situation is unknown and hence cannot be corrected

for). The wide dose-response linearity of the system is an advantage since dose distributions around PDR and HDR  $^{192}\text{Ir}$  sources can be measured for sources of clinical strength and dosimeters can be irradiated at different distances from the source(s) within one irradiation. Before the lithium formate EPR dosimetry system can be used for experimental verification of absorbed dose distributions around single sources or in other situations where dose gradients are steeper than in the present work, methods of producing and measuring with smaller dosimeters must be developed to keep the volume averaging correction reasonably low in situations with steep dose gradients such as those close ( $<3$  cm) to a single source.

## ACKNOWLEDGMENTS

This work was supported by grants from the Swedish Cancer Foundation (CF), Contract No. 07 0621. Great thanks to Sara Olsson, Håkan Hedtjärn, and Peter Larsson at Linköping University Hospital, to Emil Bengtsson and Marie Lundell at Karolinska University Hospital for their assistance in irradiating the dosimeters, and to Bengt Frost (Linköping University Hospital) for producing the PMMA phantom. Alexandr Malusek at Linköping University is acknowledged for calculating the  $f_{\text{vol}}$  factors, the uncertainty in correction factor  $D_{w,\text{phan}}(r)/\bar{D}_{w,\text{phan}}(r)$  and for valuable comments to the manuscript.

<sup>a)</sup>Electronic mail: asa.carlsson-tedgren@imv.liu.se

- <sup>1</sup>J. Lambert, T. Nakano, S. Law, J. Elsey, D. R. McKenzie, and N. Suchowerska, "In vivo dosimeters for HDR brachytherapy: A comparison of a diamond detector, MOSFET, TLD, and scintillator detector," *Med. Phys.* **34**, 1759–1765 (2007).
- <sup>2</sup>Z. Qi, X. Deng, S. Huang, J. Lu, M. Lerch, D. Cutajar, and A. Rosenfeld, "Verification of the plan dosimetry for high dose rate brachytherapy using metal-oxide-semiconductor field effect transistor detectors," *Med. Phys.* **34**, 2007–2013 (2007).
- <sup>3</sup>M. J. Rivard, B. M. Coursey, L. A. DeWerd, W. F. Hanson, M. S. Huq, G. S. Ibbott, M. G. Mitch, R. Nath, and J. F. Williamson, "Update of AAPM Task Group No. 43 Report: A revised AAPM protocol for brachytherapy dose calculations," *Med. Phys.* **31**, 633–674 (2004).
- <sup>4</sup>Z. Li, R. K. Das, L. A. DeWerd, G. S. Ibbott, A. S. Meigooni, J. Pérez-Calatayud, M. J. Rivard, R. S. Sloboda, and J. F. Williamson, "Dosimetric prerequisites for routine clinical use of photon emitting brachytherapy sources with average energy higher than 50 keV," *Med. Phys.* **34**, 37–40 (2007).
- <sup>5</sup>A. S. Meigooni, S. Sabnis, and R. Nath, "Dosimetry of palladium-103 brachytherapy sources for permanent implants," *Endocrine Hypertherm Oncol.* **6**, 107–117 (1990).
- <sup>6</sup>S.-T. Chiu-Tsao and L. L. Anderson, "Thermoluminescent dosimetry for  $^{103}\text{Pd}$  seeds (model 200) in solid water phantom," *Med. Phys.* **18**, 449–452 (1991).
- <sup>7</sup>R. Nath, A. S. Meigooni, P. Muench, and A. Melillo, "Anisotropy functions for  $^{103}\text{Pd}$ ,  $^{125}\text{I}$  and  $^{192}\text{Ir}$  interstitial brachytherapy sources," *Med. Phys.* **20**, 1465–1473 (1993).
- <sup>8</sup>C. A. Carlsson and G. Alm Carlsson, "Proton dosimetry: Measurement of depth doses from 185-MeV protons by means of thermoluminescent LiF," *Radiat. Res.* **42**, 207–219 (1970).
- <sup>9</sup>A. A. Nunn, S. D. Davis, J. A. Micka, and L. A. De Werd, "LiF: Mg, Ti TLD response as a function of photon energy for moderated filtered x-ray spectra in the range 20–250 kVp relative to  $^{60}\text{Co}$ ," *Med. Phys.* **35**, 1859–1869 (2008).
- <sup>10</sup>A. S. Kirov, J. F. Williamson, A. S. Meigooni, and Y. Zhu, "TLD, diode and Monte Carlo dosimetry of an  $^{192}\text{Ir}$  source for high dose-rate brachytherapy," *Phys. Med. Biol.* **40**, 2015–2036 (1995).
- <sup>11</sup>S. K. Olsson, E. S. Bergstrand, Å. K. Carlsson, E. O. Hole, and E. Lund, "Radiation dose measurements with alanine/agarose gel and thin alanine films around a  $^{192}\text{Ir}$  brachytherapy source, using ESR spectroscopy," *Phys. Med. Biol.* **47**, 1333–1356 (2002).
- <sup>12</sup>C. S. G. Calcina, A. De Almeida, J. R. Oliveira Rocha, F. Chen Abrego, and O. Baffa, "Ir-192 HDR transit dose and radial dose function determination using alanine/EPR dosimetry," *Phys. Med. Biol.* **50**, 1109–1117 (2005).
- <sup>13</sup>B. Ciesielski, K. Schultka, A. Kobierska, R. Nowak, and Z. Peimel-Stuglik, "In vivo alanine/EPR dosimetry in daily clinical practice: A feasibility study," *Int. J. Radiat. Oncol., Biol., Phys.* **56**, 899–905 (2003).
- <sup>14</sup>D. F. Regulla and U. Deffner, "Dosimetry by ESR spectroscopy of alanine," *Appl. Radiat. Isot.* **33**, 1101–1114 (1982).
- <sup>15</sup>T. P. Y. Wong, W. Fernando, P. N. Johnston, and I. F. Bubbs, "Transit dose of an Ir-192 high dose rate brachytherapy stepping source," *Phys. Med. Biol.* **46**, 323–331 (2001).
- <sup>16</sup>K. T. Bastin, M. B. Podgorsak, and B. R. Thomadsen, "Transit dose component of high dose rate brachytherapy: Direct measurements and clinical implications," *Int. J. Radiat. Oncol., Biol., Phys.* **26**, 695–702 (1993).
- <sup>17</sup>P. V. Houdek, J. G. Schwade, X. Wu, V. Pisciotta, J. A. Fiedler, C. F. Serago, A. M. Markoe, A. A. Abitbol, A. A. Lewin, P. G. Braunschweiler, and M. D. Sklar, "Dose determination in high dose rate brachytherapy," *Int. J. Radiat. Oncol., Biol., Phys.* **24**, 795–801 (1992).
- <sup>18</sup>R. K. Valicenti, A. S. Kirov, A. S. Meigooni, V. Mishra, R. K. Das, and J. F. Williamson, "Experimental validation of Monte Carlo dose calculations about a high-intensity Ir-192 source for pulsed dose-rate brachytherapy," *Med. Phys.* **22**, 821–829 (1995).
- <sup>19</sup>H. Gustafsson, Ph.D. thesis, Linköping University, 2008 (online, available at <http://urn.kb.se/resolve?urn=urn:nbn:se:liu:diva-11099>).
- <sup>20</sup>T. A. Vestad, E. Malinen, A. Lund, E. O. Hole, and E. Sagstuen, "EPR dosimetric properties of formates," *Appl. Radiat. Isot.* **59**, 181–188 (2003).
- <sup>21</sup>T. A. Vestad, H. Gustafsson, A. Lund, E. O. Hole, and E. Sagstuen, "Radiation-induced radicals in lithium formate monohydrate ( $\text{LiHCO}_2 \cdot \text{H}_2\text{O}$ ). EPR and ENDOR studies of X-irradiated crystal and polycrystalline samples," *Phys. Chem. Chem. Phys.* **6**, 3017–3022 (2004).
- <sup>22</sup>T. A. Vestad, E. Malinen, D. R. Olsen, E. O. Hole, and E. Sagstuen, "Electron paramagnetic resonance (EPR) dosimetry using lithium formate in radiotherapy: Comparison with thermoluminescence (TL) dosimetry using lithium fluoride rods," *Phys. Med. Biol.* **49**, 4701–4715 (2004).
- <sup>23</sup>E. Malinen, E. Waldeland, E. O. Hole, and E. Sagstuen, "The energy dependence of lithium formate EPR dosimeters for clinical electron beams," *Phys. Med. Biol.* **52**, 4361–4369 (2007).
- <sup>24</sup>H. Gustafsson, E. Lund, and S. Olsson, "Lithium formate EPR dosimetry for verification of calculated dose distributions prior to intensity modulated radiation therapy," *Phys. Med. Biol.* **53**, 4667–4682 (2008).
- <sup>25</sup>B. Schaeken and P. Scalliet, "One year of experience with alanine EPR dosimetry in radiotherapy," *Appl. Radiat. Isot.* **47**, 1177–1182 (1996).
- <sup>26</sup>IAEA, "Absorbed dose determination in external beam radiotherapy: An international code of practice based on Standards of absorbed dose to water," *Report No. IAEA TRS 398* (Vienna, International Atomic Energy Agency, 2000).
- <sup>27</sup>J. P. Seuntjens, M. Olivares, M. Evans, and E. Podgorsak, "Absorbed dose to water reference dosimetry using solid phantoms in the context of absorbed-dose protocols," *Med. Phys.* **32**, 2945–2953 (2005).
- <sup>28</sup>J. Orear, "Least squares when both variables have uncertainties," *Am. J. Phys.* **50**, 912–916 (1982).
- <sup>29</sup>V. Nagy, "Accuracy considerations in EPR dosimetry," *Appl. Radiat. Isot.* **52**, 1039–1050 (2000).
- <sup>30</sup>F. Ballester, V. Puchades, J. L. Lluch, M. A. Serrano-Andrés, Y. Limami, J. Calatayud-Pérez, and E. Casal, "Technical note: Monte-Carlo dosimetry of the HDR 12i and Plus  $^{192}\text{Ir}$  sources," *Med. Phys.* **28**, 2586–2591 (2001).
- <sup>31</sup>P. Karaiskos, A. Angelopoulos, E. Pantelis, P. Papagiannis, L. Sakelliou, E. Kouwenhoven, and D. Baltas, "Monte Carlo dosimetry of a new  $^{192}\text{Ir}$  pulsed dose rate brachytherapy source," *Med. Phys.* **30**, 9–16 (2003).
- <sup>32</sup>T. E. Burlin, in *Radiation Dosimetry*, edited by F. H. Attix and W. C. Roesch (Academic, New York, 1968), Vol. 1, p. 331.
- <sup>33</sup>I. Kawrakow and D. W. O. Rogers, "The EGSnrc Code System: Monte Carlo Simulation of Electron and Photon Transport" In: *NRCC PIRS-701* (Ottawa:National Research Council Canada, 2006).
- <sup>34</sup>D. W. O. Rogers, I. Kawrakow, J. P. Seuntjens, B. R. B. Walters, and E. Mainegra-Hing, "NRC User Codes for EGSnrc," In: *NRCC PIRS-*

- 702(revB) (Ottawa:National Research Council Canada, 2005).
- <sup>35</sup>R. Mohan, C. Chui, and L. Lidofsky, "Energy and angular distributions of photons from medical linear accelerators," *Med. Phys.* **12**, 592–597 (1985).
- <sup>36</sup>M. J. Berger, J. S. Coursey, M. A. Zucker, and J. Chang, *ESTAR, PSTAR, and ASTAR: Computer Programs for Calculating Stopping-Power and Range Tables for Electrons, Protons, and Helium Ions* (version 1.2.3), National Institute of Standards and Technology, Gaithersburg, MD, 2005. [Online] Available: <http://physics.nist.gov/Star> [January 23, 2009]. Originally published as M. J. Berger, NISTIR 4999, National Institute of Standards and Technology, Gaithersburg, MD (1993).
- <sup>37</sup>J. H. Hubbell and S. M. Seltzer, *Tables of X-Ray Mass Attenuation Coefficients and Mass Energy-Absorption Coefficients* (version 1.4) (2004). [Online] Available: <http://physics.nist.gov/xaamdi> [January 23, 2009]. National Institute of Standards and Technology, Gaithersburg, MD. Originally published as NISTIR 5632, National Institute of Standards and Technology, Gaithersburg, MD (1995).
- <sup>38</sup>Å. Carlsson Tedgren and G. Alm Carlsson, "Influence of phantom material and dimensions on experimental  $^{192}\text{Ir}$  dosimetry," *Med. Phys.* **36**, 2228–2235 (2009).
- <sup>39</sup>J. Borg and D. W. O. Rogers, "Monte Carlo simulations of photon spectra in air from  $^{192}\text{Ir}$  sources," In: *NRCC PIRS-629r* (Ottawa:National Research Council Canada, 1999).
- <sup>40</sup>D. Granero, J. Pérez-Calatayud, M. Pujades-Claumarchirant, F. Ballester, C. Melhus, and M. J. Rivard, "Equivalent phantom sizes and shapes for brachytherapy dosimetric studies of  $^{192}\text{Ir}$  and  $^{137}\text{Cs}$ ," *Med. Phys.* **35**, 4872–4877 (2008).
- <sup>41</sup>A. C. Genz and A. A. Malik, "An adaptive algorithm for numerical integration over an N-dimensional rectangular region," *J. Comput. Appl. Math.* **6**, 295–302 (1980).
- <sup>42</sup>R. Brun and F. Rademakers, "ROOT-An object oriented data analysis framework, Proceedings AIHENP'96 Workshop, Lausanne, Sep. 1996," *Nucl. Instrum. Methods Phys. Res. A* **389**, 81–86 (1997).
- <sup>43</sup>International Organization for Standardization, *Guide to the Expression of Uncertainties in Measurements*, 1995.
- <sup>44</sup>M. Anton, "Uncertainties in alanine/EPR dosimetry at the Physikalisch-Technische Bundesanstalt," *Phys. Med. Biol.* **51**, 5419–5440 (2006).
- <sup>45</sup>D. Granero, J. Pérez-Calatayud, and F. Ballester, "Monte Carlo study of the dose rate distributions for the Ir2.A85-2 and Ir2.A85-1 Ir-192 after-loading sources," *Med. Phys.* **35**, 1280–1287 (2008).